Reprinted from JOURNAL OF APPLIED PHYSICS, Vol. 41, No. 13, 5274–5278, December 1970

Raman Spectra of α Quartz Under Uniaxial Stress*

Y. D. HARKER,† C. Y. SHE, AND DAVID F. EDWARDS
Physics Department, Colorado State University, Fort Collins, Colorado 80521
(Received 11 March 1970)

The experimental results of the stress-dependent frequency and linewidth of two E and three A_1 Raman active vibrations in α quartz are reported and their behavior is qualitatively discussed. The observed nonmonotonic frequency dependence of the stress induced shifts of the A_1 lines can be understood based on the proposed modified valence-force model that includes the effects of an anharmonic potential and the applied stress.

I. INTRODUCTION

The binding or interatomic forces in solids are dependent on the electronic structure surrounding the atoms. The application of a uniaxial stress, a temperature change, or an intense laser pulse might be expected to change the electronic structure in a crystal and thereby alter the interatomic forces. This alteration might be indicated by a change in the characteristic frequencies of a vibrational mode, a change in the phonon lifetime, and thus a change in linewidth, or the induced electronic polarizability might be effected causing a change in the line intensity. Each of these effects were measured. The Raman line position and width were reported and discussed for five Raman lines in α quartz as a function of the applied stress[1] and the measured line position shifts of the A_1 lines were compared with changes predicted by a modified valence-force model developed for this purpose. The stress-dependent intensities were also measured but are not reported here.

Quartz at room temperature is a complex crystal with nine atoms per unit cell; both symmetry arguments and a detailed Raman study[2] suggest that there are $4A_1$- and $8E$-Raman active optical phonon modes in α quartz. Among the models of the α quartz,[3,4] the valence-force model proposed by Kleinman and Spitzer[3] gives the most details for the symmetric A_1 modes; they reported both calculated eigenvalues and eigenvectors for these modes. The valence-force model assumes three types of interactions: (1) the Si–O bond-stretching potential; (2) the O–Si–O angle-bending potential; and (3) Si–O–Si angle-bending potential. In the harmonic approximation as assumed by Kleinman and Spitzer, the interactions are

$$V_s=\tfrac{1}{2}\kappa\sum_{\rho}[(\mathbf{x}_\rho-\mathbf{x}_\rho')\cdot\hat{\rho}]^2, \tag{1}$$

$$V_{b,\mathrm{Si}}=\tfrac{1}{2}\kappa'\sum_{\mathrm{Si}}(\Delta\cos\theta)^2d^2, \tag{2}$$

and

$$V_{b,\mathrm{O}}=\tfrac{1}{2}\kappa''\sum_{\mathrm{O}}(\Delta\cos\theta)^2d^2, \tag{3}$$

where

$$\Delta\cos\theta=d^{-1}[\hat{\rho}-(\hat{\rho}\cdot\hat{\rho}')\hat{\rho}']\cdot(\mathbf{x}_\rho'-\mathbf{x})+d^{-1}[\hat{\rho}'-(\hat{\rho}\cdot\hat{\rho}')\hat{\rho}]\cdot(\mathbf{x}_\rho-\mathbf{x}), \tag{4}$$

where $\hat{\rho}$ is the unit vector representing the bond direction, κ, κ', and κ'' are "spring constants," d is the nearest-neighbor silicon-to-oxygen distance and $\mathbf{x}$ is the displacement of either the Si or O atom. The summation in (1) is over all nearest-neighbor bonds with one end terminating on a silicon atom in the unit cell and the summations in (2) and (3) are over all bond angles at each silicon and oxygen atom within the unit cell, respectively. Using (1)–(4), Kleinman and Spitzer solved for the normal-mode vectors and frequencies for the four totally symmetric modes and then adjusted the "spring constants" to give the best fit to the measured values. In modifying the valence-force model to include strain, we replace the displacement $\mathbf{x}$ by $\mathbf{x}+\mathbf{u}$ in Eqs. (1)–(3) by a method suggested by Born and Huang,[5] and we also include the lowest-order anharmonic contribution to the deformed potential. $\mathbf{u}$ is the total displacement due to a homogeneously strained lattice which contains both microscopic- and macroscopic-strain contributions. The anharmonic

valence–force potentials may be expressed as

$$V_s^{(3)} = \Phi_s^{(3)} \sum_{\rho} [(\mathbf{x}_\rho' - \mathbf{x}_\rho) \cdot \hat{\rho}]^3, \quad (5)$$

$$V_{b,\mathrm{Si}}^{(3)} = \Phi_{b,\mathrm{Si}}^{(3)} \sum_{\mathrm{Si}}' (\Delta \cos\theta)^3 d^3, \quad (6)$$

and

$$V_{b,\mathrm{O}}^{(3)} = \Phi_{b,\mathrm{O}}^{(3)} \sum_{\mathrm{O}} (\Delta \cos\theta)^3 d^3, \quad (7)$$

where the $\Phi^{(3)}$'s are third-order elastic-force constants. The microscopic or internal strains represent the atomic displacements necessary to minimize the deformation energy; their values were determined for the valence-force model.[6] The resulting stress dependent potential, including the above anharmonic contributions, was calculated up to first order in $\mathbf{u}$ and second order in $\mathbf{x}$ in terms of the normal-mode coordinates of A_1 modes given by Kleinman and Spitzer. The changes in the normal-mode frequencies produced by this stress dependent potential are evaluated using first-order perturbation theory[6] and the results for the four A_1 modes are the following:

$$\Delta\bar{\nu}_1(207\ \mathrm{cm}^{-1}) = 3.96\times10^{-4}Y_y \times(-8.25\times10^{-4}\kappa - 5.21\times10^{-3}\kappa' + 2.91\times10^{-3}\kappa'' + 9.98\times10^{-14}\Phi_s^{(3)} - 1.49\times10^{-10}\Phi_{b,\mathrm{Si}}^{(3)} - 3.87\times10^{-11}\Phi_{b,\mathrm{O}}^{(3)}), \quad (8a)$$

$$\Delta\bar{\nu}_2(352\ \mathrm{cm}^{-1}) = 2.72\times10^{-4}Y_y \times(-7.46\times10^{-4}\kappa - 5.20\times10^{-3}\kappa' + 2.78\times10^{-3}\kappa'' + 3.10\times10^{-14}\Phi_s^{(3)} + 2.36\times10^{-10}\Phi_{b,\mathrm{Si}}^{(3)} - 1.51\times10^{-10}\Phi_{b,\mathrm{O}}^{(3)}), \quad (8b)$$

$$\Delta\bar{\nu}_3(466\ \mathrm{cm}^{-1}) = 1.68\times10^{-4}Y_y(-1.93\times10^{-3}\kappa + 1.40\times10^{-2}\kappa' + 1.93\times10^{-3}\kappa'' + 5.54\times10^{-13}\Phi_s^{(3)} + 3.98\times10^{-11}\Phi_{b,\mathrm{Si}}^{(3)} - 6.72\times10^{-10}\Phi_{b,\mathrm{O}}^{(3)}), \quad (8c)$$

$$\Delta\bar{\nu}_4(1081\ \mathrm{cm}^{-1}) = 7.88\times10^{-5}Y_y \times(3.77\times10^{-3}\kappa - 8.65\times10^{-3}\kappa' - 1.88\times10^{-3}\kappa'' + 9.10\times10^{-12}\Phi_s^{(3)} - 7.10\times10^{-14}\Phi_{b,\mathrm{Si}}^{(3)} - 1.87\times10^{-11}\Phi_{b,\mathrm{O}}^{(3)}), \quad (8d)$$

where Y_y is the stress (in units of 10^9 dyn/cm^2) applied to the y face of the crystal in the direction parallel to the y axis.

The above calculation is consistent with the discussion of strain given in Born and Huang and the details are given elsewhere.[6] Equation (8) will be used later to demonstrate the nonmonotonic frequency dependence of the stress-induced shifts of the A_1 lines in α quartz.

II. RAMAN SPECTROMETER SYSTEM

The Raman spectrometer system used for these experiments has been described in detail elsewhere[7] and is similar in many aspects to that described by Ducros and Olivie.[8] A 50-mW He–Ne laser operating with a uniphase output is used as the excitation source. The active volume of the sample as determined by the laser focusing lens, is imaged (1:1) onto the entrance slit of a grating monochromator. The scattered radiation flux reaching the photodetector[9] is such that photon counting techniques can be used with the advantage that the output data are in digital form and is therefore directly compatible with a computer for analysis. A multichannel analyzer is used for collecting the output data as well as for controlling the step-wavelength drive of the monochromator. The instrument width of this system is comparable with the Raman linewidths so that a deconvolution procedure is necessary to obtain the true lineshapes. For the spectrometer system used, this deconvolution is done by computer giving the true line position, width, and intensity.

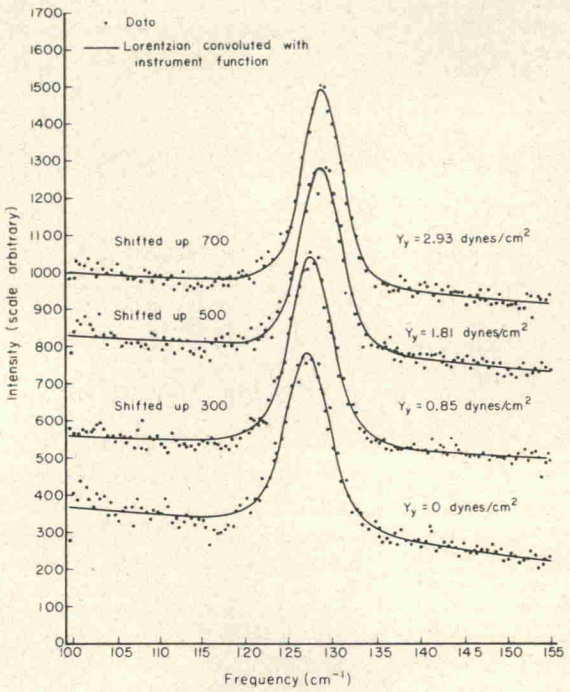

FIG. 1. Experimental raw data for the 128-cm^{-1} line. For clarity the curves have been shifted in the vertical direction as indicated. The curves through the data points are least-squares fits of Lorentzian functions convoluted with the instrument function.

The samples used for these experiments were synthetic quartz from several sources as well as natural quartz also from several sources. Within the accuracy of our measurements the effects observed were not dependent on the sample origin. The results described in the following section were for a sample cut from a synthetically grown crystal. Each sample, 0.55×0.55×2.14 cm, was free from twinning and the impurity concentration was approximately 30 ppm by weight. The long dimension of the sample was parallel to the crystallographic x axis and the stress was applied

TABLE I. Comparison of calculated and observed values of the first derivatives of line position versus applied stress.

Mode ν_0 (cm^{-1})	κ[a]	κ/κ'	κ''/κ'	$\Phi_s^{(3)}$ [b]	$\Phi_{b,Si}^{(3)}$	$\Phi_{b,O}^{(3)}$	$(\partial\nu/\partial Y_y)_{calc}$ (cm^{-1}/kbar)	$(\partial\nu/\partial Y_y)_{obs}$ (cm^{-1}/kbar)	$(\partial\nu/\partial P)_{obs}$[c] ($cm^{-1}$/kbar)
207							0.326	1.28±0.06	1.6–2.1
352							0.021	−0.05±0.06	−0.2–+0.3
	4.32	15	0	2	2	0.5			
466							0.132	0.44±0.12	1.2–0.9
1081							−0.109		−0.2–0.4
207							1.28		
352							−0.80		
	4.32	15	0	···	17.2	4.3			
466							0.44		
1081									
207							1.28		
352							−0.56		
	4.32	10	−2.2	···	14.8	4.2			
466							0.44		
1081									
207							1.28		
352							−0.85		
	4.32	16	1	···	17.7	4.4			
466							0.44		
1081									

[a] κ's are in units of 10^5 dyn/cm.
[b] Φ's are in units of 10^{12} dyn/cm^2, and the value of $\Phi_s^{(3)}$ within this order-of-magnitude will not affect the calculated results listed.
[c] Asell and Nicol, Ref. 15, hydrostatic pressure.

parallel to the y axis. The incident light was in the x direction and the scattered light was observed along the z axis. The stress was applied by placing the sample between the jaws of a hydraulic press. The scattering volume was approximately a cylinder 4 mm×50 μ in diameter which is a small fraction of the total sample volume and thus the applied stress across the scattering volume was considered to be uniform.

III. EXPERIMENTAL RESULTS

The Stokes components of the Raman spectra were measured for five of the more intense lines in quartz as a function of applied stress. The line position, width, and intensity were measured for each line. Shown in Fig. 1 are examples of the raw data for the 128-cm^{-1} line illustrating the importance of the deconvolution procedure to finding the true linewidth values. From this figure the change in line position with applied stress is apparent but the change in linewidth is apparent only after the deconvolution of the true line shape with the instrument function.

The uniaxial stress measurements were made for increasing as well as decreasing pressures and showed no hysteresis effects. The stress dependence of the line positions and linewidths are shown in Figs. 2 and 3 for the five lines measured. The intensity data were also measured for these five lines but are not shown. For the 128-cm^{-1} line both the Stokes and the anti-Stokes components were measured. The stress-dependent 128-cm^{-1} anti-Stokes line positions which are

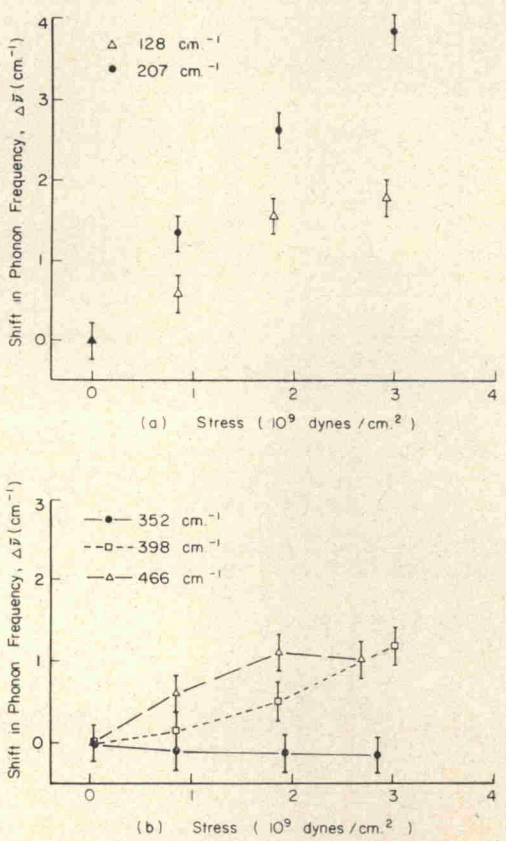

FIG. 2. Shift in phonon frequency versus applied stress. In (b) the points have been connected for clarity.

not shown behave similarly to the 128-cm^{-1} Stokes data.

From Fig. 2 it can be seen that the line positions increase with applied stress for all the lines except the 352-cm^{-1} line which is approximately independent of stress. The linewidths shown in Fig. 3 are seen to initially decrease with stress. The effects of the applied stress on the line position and width are similar to that observed for decreasing sample temperature.[10–12] The increase in frequency as the sample is compressed is what might be expected since the atoms become more closely packed making it more difficult for each atom to move. The phonon lifetimes are affected by multiphonon interactions induced by the strain resulting from the applied stress; various possible strain-induced multiphonon interactions have been formally considered in the literature.[13] For no change in sample temperature, the increase in phonon frequency would lower the associated phonon population available for the multiphonon interactions. The population effect, perhaps of minor importance, should be included in the linewidth considerations.

Using Eq. (8) the stress-induced changes in line frequency were calculated for the four A_1 modes and the results were compared with the slopes found from Fig. 2. The results are listed in Table I for different

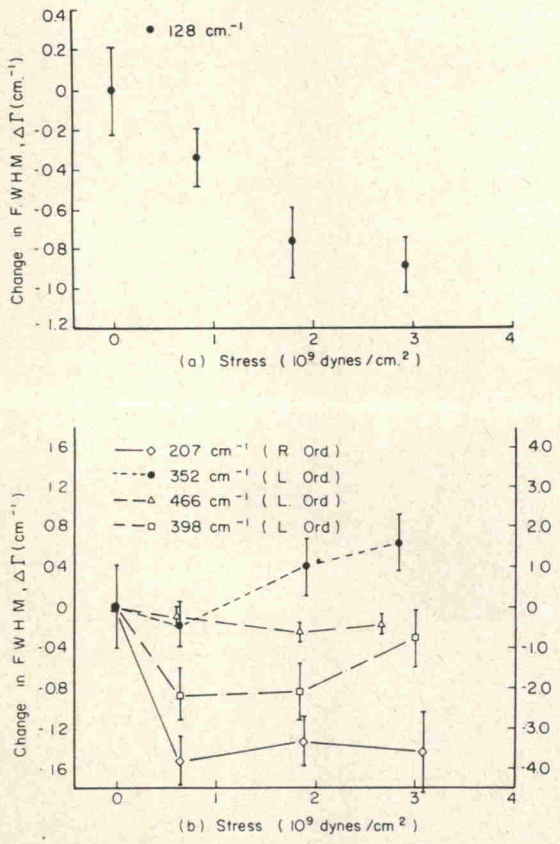

FIG. 3. Change in the full width at half-maximum versus stress. The data points have been connected for clarity.

combinations for the constants κ, κ', κ'', $\Phi_s^{(3)}$, $\Phi_{b,Si}^{(3)}$, and $\Phi_{b,O}^{(3)}$. The first values listed were calculated using the κ's as given by Kleinman and Spitzer. The third-order Φ coefficients were estimated from ultrasonic third-order elasticity measurements.[14] The elastic coefficients are defined to be identical with those encountered in anharmonic lattice theory and are proportional to the third-order coefficients in Eq. (8). Exact data for the Φ's could not be found but their values will in general be of the same order-of-magnitude (10^{12} dyn/cm^2). For this reason the strain effects were evaluated for several values of the Φ's. The combinations listed in Table I were chosen to demonstrate the relative sensitivity of the magnitude of the different coefficients on the calculated slopes. From the table it can be seen that the value of $(\partial\nu/\partial Y_y)$ is insensitive to the choice of $\Phi_s^{(3)}$ for all of the A_1-vibrations. For the 352-cm^{-1} vibration the coefficient $\Phi_{b,O}^{(3)}$ is very sensitive because of the cancellation of the contributions due to $\Phi_{b,Si}^{(3)}$ with that due to the κ's as can be seen from Eq. (8). The 1081-cm^{-1} mode depends on all three values for the Φ's and is the only mode for which the third-order stretching coefficient $\Phi_s^{(3)}$ is of some importance. The stress dependence on the position of the 1081-cm^{-1} line was not measured because the line was too weak.

By way of comparison Asell and Nicol[15] have measured the effect of hydrostatic pressure on the A_1- and E-mode Raman line position for pressures up to about 40 kbar. Comparing their data for the four A_1 lines and the 128- and 398-cm^{-1} E lines it is seen that the agreement is quite good considering the rather large error bars on the Asell–Nicol data.

IV. CONCLUSIONS

The results of this research indicate that quantitative Raman scattering can be used as an effective tool for detecting and analyzing the effects of homogeneous strains in crystalline quartz. The valence-force model used for calculating normal-mode frequencies was modified by including the effects of an anharmonic potential and applied stress. As a consequence, the observed nonmonotonic stress-induced changes in frequency for the four A_1 modes in quartz can be understood with reasonable accuracy.

An apparent correlation is observed between the stress and temperature dependence[10] of the line position for the five lines measured here and is consistent with the observations made by Asell and Nicol. The sample volume change under uniaxial stress is smaller than that produced by the hydrostatic pressure experiments. Our modified valence-force model indicates that the stress dependence of the phonon frequencies depend on individual normal-mode vibration and probably is not a simple volume dependence as suggested by Asell and Nicol.

Using the order-of-magnitude values for the third-order elastic constants the modified valence-force

model has been able to demonstrate the non-monotonic dependence of frequency shift with line frequency for modes belonging to the same symmetry species. The set of coefficients, κ and Φ, giving the best correspondence with the measured values are those listed first in Table I. The nonmonotonic dependence of frequency shifts and the insensitiveness of the $\Phi_s^{(3)}$ suggest that the frequency shift depends mainly on the way the constituent atoms, especially the oxygens in this case, move in a normal-mode vibration. The comparison of the calculated slopes and the measured ones in the first row of Table I is quite good, considering the kind of accuracy one may expect even in the calculation of the second-order elastic constants.[16]

* This work was supported in part by a contract with the Air Force Cambridge Research Laboratories, Office of Aerospace Research, USAF.

† NDEA Fellow; present address: Idaho Nuclear Corporation, Idaho Falls, Ida. 83401.

[1] Y. D. Harker, C. Y. She, and D. F. Edwards, Appl. Phys. Lett. **15**, 272 (1969).
[2] J. D. Masso, C. Y. She, and D. F. Edwards, Phys. Rev. **B1**, 4179 (1970).
[3] D. A. Kleinman and W. G. Spitzer, Phys. Rev. **125**, 16 (1962).
[4] M. M. Elcombe, Proc. Phys. Soc. (London) **91**, 947 (1967).
[5] M. Born and K. Huang, *Dynamical Theory of Crystal Lattices* (Clarendon, Oxford, 1954).
[6] Y. D. Harker, Ph.D. dissertation, Department of Physics, Colorado State University, 1969.
[7] J. D. Masso, Y. D. Harker, and D. F. Edwards, J. Chem. Phys. **50**, 5420 (1969).
[8] A. Ducrcs and M. Olivie, Electron. Ind. **119**, 801 (1968).
[9] Y. D. Harker, J. D. Masso, and D. F. Edwards, Appl. Opt. **8**, 2563 (1969).
[10] T. M. K. Nedungadi, Proc. Indian Acad. Sci **11**, 86 (1940).
[11] P. K. Narayanaswany, Proc. Indian Acad. Sci. **26**, 521 (1947).
[12] A. S. Pine and P. E. Tannenwald, Phys. Rev. **178**, 1424 (1969).
[13] R. A. Cowley, Advan. Phys. **12**, 421 (1963).
[14] R. N. Thurston, H. J. McSkimin, and P. Andreatch, Jr., J. Appl. Phys. **37**, 267 (1967).
[15] J. F. Asell and M. Nicol, J. Chem. Phys. **49**, 5395 (1968).
[16] C. L. Julian and F. O. Lane, Jr., J. Appl. Phys. **39**, 3931 (1968).